ACS Chemical Neuroscience

Article

Multifunctional analogs of kynurenic acid for the treatment of Alzheimer's disease: Synthesis, pharmacology and molecular modeling studies

Girdhar Singh Deora, Srinivas Kantham, Stephen Chan, SATISH NATHA N DIGHE, Suresh K. Veliyath, Gawain McColl, Marie-Odile Parat, Ross Peter McGeary, and Benjamin P. Ross

ACS Chem. Neurosci., **Just Accepted Manuscript** • DOI: 10.1021/acschemneuro.7b00229 • Publication Date (Web): 21 Aug 2017

ACS Publications

ACS Chemical Neuroscience is published by the American Chemical Society. 1155 Sixteenth Street N.W., Washington, DC 20036

Multifunctional analogs of kynurenic acid for the treatment of Alzheimer's disease: Synthesis, pharmacology and molecular modeling studies

Girdhar Singh Deora,[†] Srinivas Kantham,[†] Stephen Chan,[†] Satish N. Dighe,[†] Suresh K. Veliyath,[†] Gawain McColl,[‡] Marie-Odile Parat,[†] Ross P. McGeary,[#] and Benjamin P. Ross[†,*]

[†]The University of Queensland, School of Pharmacy, Brisbane, Queensland 4072, Australia.

[‡]The Florey Institute of Neuroscience and Mental Health, University of Melbourne, Victoria 3010, Australia.

[#]The University of Queensland, School of Chemistry and Molecular Biosciences, Brisbane, Queensland 4072, Australia.

KEYWORDS. Alzheimer's disease, NMDAR antagonist, mGluR5 antagonist, Acetylcholinesterase inhibitor, Antioxidant, Amyloid beta peptide.

ABSTRACT: We report the synthesis and pharmacological investigation of analogs of the endogenous molecule kynurenic acid (KYNA) as multifunctional agents for the treatment of Alzheimer's disease (AD). Synthesized KYNA analogs were tested for their *N*-methyl-D-aspartate (NMDA) receptor binding, mGluR5 binding and function, acetylcholinesterase (AChE) inhibition, DPPH radical scavenging, interference with the amyloid beta peptide (Aβ) fibrillation process, and protection against Aβ-induced toxicity in transgenic *Caenorhabditis elegans* strain GMC101 expressing full-length $A\beta_{42}$. Molecular modeling studies were also performed to predict the binding modes of most active compounds with NMDAR, mGluR5 and $A\beta_{42}$. Among the synthesized analogs, **3c**, **5b** and **5c** emerged as multifunctional compounds that act *via* multiple anti-AD mechanisms including AChE inhibition, free radical scavenging, NMDA receptor binding, mGluR5 binding, inhibition of $A\beta_{42}$ fibril formation, and disassembly of preformed $A\beta_{42}$ fibrils. Interestingly, **5c** showed protection against $A\beta_{42}$-induced toxicity in transgenic *C. elegans* strain GMC101. Moreover, **5b** and **5c** displayed high permeability in an MDR1-MDCKII cell-based model of the blood-brain barrier (BBB). Compound **3b** emerged with specific activity as a micromolar AChE inhibitor, however it had low permeability in the BBB model. This study highlights the opportunities that exist to develop analogs of endogenous molecules from the kynurenine pathway for therapeutic uses.

INTRODUCTION

The *N*-methyl-D-aspartate receptor (NMDAR) is an ionotropic glutamate receptor that mediates glutamatergic neurotransmission and affects several basic functions in the central nervous system (CNS) including neurodevelopment, synaptic plasticity, learning, and memory formation.[1] For the activation of ionotropic glutamate receptors, glutamate is not the only agonist; glycine and D-serine are co-agonists and the presence of one or the other along with glutamate is needed for the receptor to function.[2] Over-activation of NMDAR causes pathological excitotoxicity that is linked to several neurodegenerative diseases, including Alzheimer's disease (AD)[3, 4] which is characterized by progressive cognitive decline and slow destruction of memory and thinking skills.[5] Kynurenic acid (KYNA), one of the first reported products of tryptophan metabolism (Scheme 1),[6] possesses neuroprotective properties by antagonizing the effect of NMDAR-mediated excitotoxicity.[7] KYNA is an endogenous competitive antagonist of ionotropic glutamate receptors, and it has a high affinity for the obligatory glycine co-agonist site of the NMDAR.[8, 9]

Chemical modification of endogenous molecules can generate new compounds with improved potencies and/or additional functions that can be of therapeutic benefit. For example, 5,7-dichlorokynurenic acid, an analog of KYNA, is one of the most potent excitatory amino acid receptor antagonists.[10] This illustrates that the introduction of substituents into the quinolone benzene ring of KYNA may improve the ligand-receptor interactions and increase the potency of this endogenous molecule. Furthermore, these substituents could also impart additional multifunctional effects that might be useful for treating AD. In this report, we describe our investigation of synthetic analogs of KYNA as prospective multifunctional agents for AD pharmacotherapy.

Symptomatic treatments are the established pharmacotherapy for AD,[11] comprising the cholinesterase inhibitors donepezil, rivastigmine, and galantamine, and the uncompetitive NMDAR antagonist memantine which blocks current flow by occupying the NMDAR ion channel.[12, 13] AD is a multifactorial disorder which is hypothesized to involve several different etiopathogenic mechanisms.[14] Consequently, multifunctional agents that

act on multiple drug targets have recently been a focus of AD drug discovery studies,[15-19] particularly agents with potential disease-modifying properties that target the formation of amyloid beta (Aβ) peptide (secretase inhibitors), deposition of Aβ (fibrillation inhibitors), deposition of tau, inflammation, and/or oxidative damage (antioxidants and metal chelators). There has also recently been interest in metabotropic glutamate receptors (mGluRs), especially mGluR5, which modulate NMDAR activity and excitotoxicity.[20, 21] Antagonists of mGluR5 are known to protect against excitotoxic neurodegeneration and Aβ-induced toxicity.[22-24]

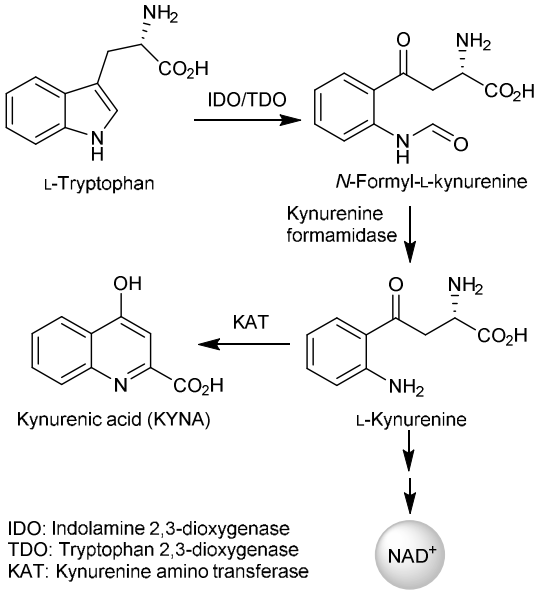

Scheme 1. Biosynthesis of kynurenic acid via tryptophan metabolism.

In this study, analogs of KYNA were investigated for multifunctional activity in relation to acetylcholinesterase (AChE) inhibition, NMDAR binding, mGluR5 binding and function, free radical scavenging, inhibition of $A\beta_{42}$ fibrillation, and $A\beta_{42}$ fibril disassembly. Furthermore, the *in vivo* protective effect of the molecules against $A\beta_{42}$-induced toxicity in transgenic *Caenorhabditis elegans* strain GMC101 was studied,[25] and the blood-brain barrier (BBB) permeability of the most active compounds was estimated using a cell-based model of the BBB. Molecular modeling studies were also performed to predict the binding modes of most active compounds with NMDAR, mGluR5 and $A\beta_{42}$.

RESULTS AND DISCUSSION

Chemistry. Scheme 2 describes the synthesis of the target KYNA analogs, which was accomplished using established synthetic approaches. Substituted dimethyl anilinofumarates (**2a-c**) were synthesized by treating substituted anilines (**1a-c**) with dimethyl acetylenedicarboxylate.[26-28] Compounds **3a-c** were formed by cyclization of **2a-c** at 120 °C in polyphosphoric acid (PPA). Hydrolysis of methyl esters **3a-c** was performed using aqueous sodium hydroxide in methanol to obtain the corresponding carboxylic acids **4a-c**. In an alternative pathway, nitroaromatics **3a-c** were reduced by catalytic hydrogenation to form anilines **5a-c**.[29, 30] The identity and purity of the synthesized compounds were determined using a combination of thin-layer chromatography, melting point, ^{1}H and ^{13}C NMR spectroscopy, high-resolution mass spectrometry and RP-HPLC (Supporting Information).

Scheme 2. Synthesis of analogs of kynurenic acid.[a]

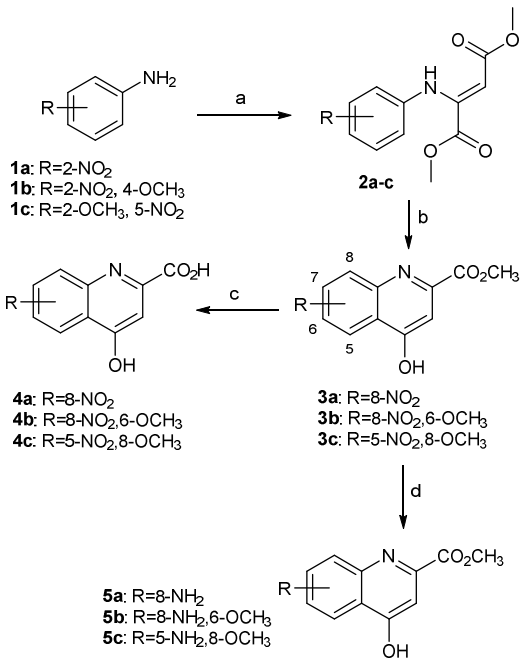

[a]Reagents and conditions: (a) Dimethyl acetylenedicarboxylate, CH_3OH, reflux, 3-5 h (64-87%); (b) PPA, 120 °C, 1 h (28-65%); (c) CH_3OH, 2 M aq. NaOH, r.t., 0.5-1 h (83-90%); (d) 5% Pd/C, H_2, CH_3OH, r.t., 4 h (40-95%).

Receptor binding affinity and function. The NMDAR binding affinity of the compounds was investigated using a radioligand binding assay (Table 1).[31, 32] All of the synthesized compounds were subjected to primary screening at 10 μM. Compounds **3b**, **3c**, **4c**, **5a,** and **5b** were weak-to-moderate inhibitors of [^{3}H]MK-801 binding to the NMDAR, with percent inhibition values ranging from 28 to 42%, though this was superior to KYNA which exhibited only 11% inhibition. Compounds **3c** and **5b** were further tested in a secondary radioligand binding assay to determine binding affinity (K_i). Compounds **3c** and **5b** exhibited K_i values of 6.27 and 7.98 μM, respectively. The NMDAR antagonist dizocilpine (MK-801) was also tested as a reference molecule and had a K_i value of 0.007 μM.

Table 1. Receptor binding affinity (NMDAR, mGluR5), function (mGluR5), and acetylcholinesterase inhibition data.

Compound	NMDAR inhibition of [^{3}H]MK-801 binding (% at 10 μM)	NMDAR binding affinity K_i (μM)	mGluR5, inhibition of [^{3}H]MPEP binding (% at 10 μM)	mGluR5 binding affinity K_i (μM)	mGluR5 antagonist function (% at 10 μM)	mGluR5 agonist function (% at 10 μM)	*Ee*AChE IC_{50} (μM) ± S.E.M.[a,b]
3a	7.64	nd[c]	46.9	nd[d]	nd[d]	nd[d]	33.6 ± 3.0
3b	28.2	nd[c]	43.9	nd[d]	nd[d]	nd[d]	10.9 ± 0.7
3c	37.9	6.27	57.3	0.885	21.9 ± 2.50	3.45 ± 1.75	11.0% at 10 μM[e]
4a	7.09	nd[c]	9.11	nd[d]	nd[d]	nd[d]	nd[f]
4b	7.29	nd[c]	28.2	nd[d]	nd[d]	nd[d]	133 ± 11
4c	30.2	nd[c]	28.0	nd[d]	nd[d]	nd[d]	nd[f]
5a	30.5	nd[c]	57.5	2.48	-3.93 ± 1.33	5.70 ± 1.31	nd[f]
5b	42.4	7.98	67.9	0.829	11.17 ± 3.90	5.17 ± 0.833	nd[f]
5c	16.0	nd[c]	-38.3	nd[d]	nd[d]	nd[d]	nd[f]
KYNA	10.8	nd[c]	35.5	nd[d]	nd[d]	nd[d]	nt
Dizocilpine (MK-801)	100	0.007	nt	nt	nt	nt	nt
Fenobam	nt	nt	100	0.069	nt	nt	nt
Rivastigmine[g]	nt	nt	nt	nt	nt	nt	76.2 ± 2.5
Tacrine[h]	nt	nt	nt	nt	nt	nt	0.107 ± 0.009
Donepezil[h]	nt	nt	nt	nt	nt	nt	0.096 ± 0.009

nd-not determined. nt-not tested. [a]Data was taken after 40 min incubation and collected from ≥3 experiments. [b]KYNA and KYNA analogs **3**-**5** were screened and only **3a**, **3b**, **3c,** and **4b** showed significant enzyme inhibition. [c]Values only provided for compounds which showed >35% inhibition of [^{3}H]Mk-801 binding at 10 μM in the primary screening assay. [d]Values only provided for compounds which showed >50% inhibition of [^{3}H]MPEP binding at 10 μM in the primary screening assay. [e]IC_{50} not determined due to solubility constraints; **3c** exhibited 34.7% inhibition at 50 μM. [f]IC_{50} was only determined for compounds which showed >10% inhibition 10 μM. [g]Rivastigmine is a pseudo-irreversible inhibitor. [h]Data for these reference drugs was recently published.[33]

To predict the binding modes of **3c** and **5b** with the glycine-binding site of the NR1 subunit of the NMDAR, molecular modeling studies were conducted. The structural coordinates of the NR1 subunit of the NMDAR were taken from protein data bank (PBD) entry 1PBQ.[34] Both **3c** and **5b** were predicted to have multiple hydrogen bonding interactions with the residues of the glycine-binding site of the NMDAR. The nitro and hydroxy groups of **3c** were predicted to form a network of hydrogen bonds with Thr126 and Arg131 (Figure 1A). Similarly, the functional groups of **5b** were expected to interact with Gln13, Pro124, Arg131, Ser180 and Asp224 via hydrogen bonds (Figure 1B). The aromatic rings of both compounds were predicted to interact *via* π-π stacking with the phenyl ring of Phe92.

The mGluR5 binding affinity of the compounds was determined using a radioligand binding assay (Table 1). All of the synthesized compounds underwent primary screening at 10 μM. Compounds **3c**, **5a,** and **5b** were moderate inhibitors of [^{3}H]MPEP binding to mGluR5 with percent inhibition values in the range of 57–68%, superior to KYNA which exhibited 35% inhibition. These compounds were then tested in a secondary radioligand binding assay, and the K_i values of **3c**, **5a,** and **5b** were 0.885, 2.48 and 0.829 μM, respectively. The mGluR5 antagonist fenobam was also tested as a reference molecule and had a K_i value of 0.069 μM. Primary screening for mGluR5 agonist or antagonist activity of **3c**, **5a,** and **5b** was conducted with 10 μM of compound (Table 1). Agonist function was reported as the percent of maximal mGlurR5 activity with a saturating concentration of agonist (glutamate) set to 100%.[31] Antagonist function was expressed as the percent inhibition of mGluR5 activity in the presence of an EC_{80} concentration of the agonist (glutamate) with a saturating concentration of

reference antagonist (MPEP) set to 100%.[31] Compound **3c** displayed relatively weak antagonism with 22% inhibition of mGluR5 activity and no appreciable agonism.

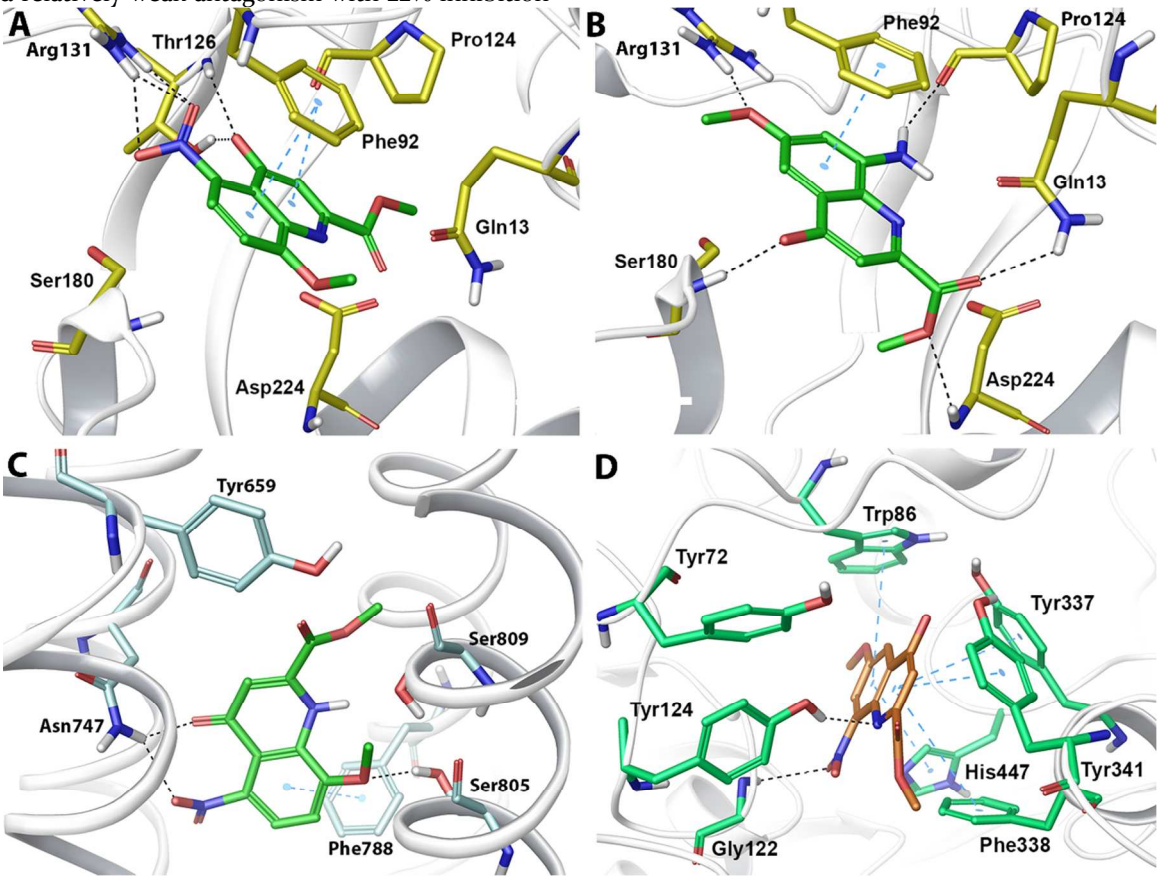

Figure 1. Docking models obtained from molecular modeling studies. (A,B) Proposed binding interactions of **3c** (A) and **5b** (B) with active site residues of the glycine-binding site of the NMDAR (PDB entry: 1PBQ). Binding site residues are depicted as sticks with carbon atoms represented in yellow (green for **3c** and **5b**). (C) Docked model of a tautomer of **3c** with mGluR5 (PDB entry: 4OO9) showing proposed binding interactions. Protein residues are represented as sticks with carbon atoms in turquoise (green for **3c**). (D) Docked model of **3b** with huAChE (PDB entry: 4EY7) showing proposed binding interactions with the active site pocket. Active site residues are represented as sticks with carbon atoms in green (orange for **3b**) The black dashed lines represent hydrogen bonds, and light blue dashed lines represent π-π stacking. In all figures, the black dashed lines represent hydrogen bonds, and light blue dashed lines represent π-π stacking between ligand and receptor.

The binding interactions of **3c** with mGluR5 were predicted by molecular modeling studies (Figure 1 C) using the structural coordinates of mGluR5 taken from PDB entry 4OO9.[35] The nitro and hydroxy groups of **3c** showed proposed hydrogen bond interactions with an amino group of Asn747. Similarly, the oxygen atom of the methoxy group of **3c** was expected to form a hydrogen bond with the hydroxyl group of Ser805, and π-π stacking between the aromatic rings of **3c** and Phe788 was also predicted.

Acetylcholinesterase inhibition. Inhibition of AChE by the synthesized KYNA analogs and reference drugs rivastigmine, tacrine and donepezil, was determined by a modified Ellman's assay method (Table 1).[36] Among all of the synthesized compounds, **3a-c** and **4b** showed substantial inhibition of *Electrophorus electricus* AChE (*Ee*AChE). Compound **3b** emerged as the most active compound among the tested compounds with an IC_{50} value of 10.9 μM followed by **3a** (IC_{50} 33.6 μM) and **3c** (34.7% inhibition at 50 μM). Compound **4b**, which is an acid derivative of ester **3b**, also inhibited the enzyme, but it was an order of magnitude weaker than **3b**, with an IC_{50} of 133 μM. These molecules were also evaluated for equine BuChE inhibition, but no significant activity was observed up to a concentration of 100 μM. Hence, these compounds appear to selectively inhibit AChE. The catalytic site of BuChE is rich in aliphatic residues and ~200 $Å^3$ larger than that of AChE, therefore, the inability of these analogs to inhibit BuChE could be due to weak binding or poor fit with the large catalytic binding site of BuChE.[33, 37]

To investigate the binding of **3b** with the active site of AChE, molecular modeling studies were performed using a reported crystal structure of human AChE (huAChE) (PDB entry 4EY7).[38] The docked model of **3b** with the

huAChE binding site is represented in Figure 1D. The oxygen atom of the nitro group and ring nitrogen of **3b** showed proposed hydrogen bond interactions with Gly122 and Tyr124, respectively. Additionally, a dense network of π-π stacking between the aromatic rings of **3b** and Trp86, Tyr337, Phe338, Tyr341, and His447 was also predicted.

DPPH radical scavenging. The compounds were tested for their free radical scavenging potential using the DPPH radical assay. The violet DPPH free radical is converted into its reduced yellow form DPPH-H by antioxidant molecules.[39] The free radical scavenging properties of the molecules were estimated from two parameters: antioxidant stoichiometry and antioxidant reactivity. The antioxidant stoichiometry is the number of DPPH radicals scavenged by one molecule of antioxidant, and the antioxidant reactivity is the rate of the reaction between the antioxidant and DPPH radicals.[40, 41]

Table 2. Antioxidant potential of the KYNA analogs with the DPPH radical[a,b]

Compounds	Antioxidant stoichiometry	Antioxidant reactivity Bimolecular rate constant[d]	
	Stoichiometric factor (n)[c]	Overall k_b (M^{-1} s^{-1})	Stoichiometric k'_b (M^{-1} s^{-1})[e]
5a	2.75 ± 0.05	142 ± 8	51.9 ± 3.1
5b	3.17 ± 0.06	574 ± 45	181 ± 11
5c	2.39 ± 0.04	2384 ± 180	1017 ± 92
EGCG	15.1 ± 0.2	3486 ± 34	232 ± 4
GA[f]	6.30 ± 0.18	1335 ± 316	212 ± 56

[a]KYNA and KYNA analogs **3-5** were tested, and only **5a-c** were active. [b]Data are expressed as the mean ± SEM of at least three independent experiments. [c]Number of DPPH molecules reduced by one molecule of compound in 24 h. [d]R^2 values of plots of $(dA/dt)_o$ vs. A_o[AH] were between 0.85 and 0.99. [e]$k'_b = k_b/n$. [f]This antioxidant data was recently published.[40]

(-)-Epigallocatechin gallate (EGCG) and gallic acid (GA) were tested as reference antioxidant compounds. ECCG and GA are naturally occurring polyphenolic compounds found in tea and previously reported by us and others for their free radical scavenging properties.[40, 42] EGCG had an overall bimolecular rate constant (k_b) of 3486 M^{-1} s^{-1} and a stoichiometric factor (n) of 15.1. No significant activity was observed for **3a-c** and **4a-c**, but all three amino-substituted KYNA analogs **5a-c** showed substantial radical scavenging activity (Table 2). Among these analogs, **5c** had comparatively faster reaction kinetics with a k_b value of 2384 M^{-1} s^{-1} and an antioxidant stoichiometric factor of 2.39, resulting in a k'_b value (k_b/n) of 1017 M^{-1} s^{-1}, which is fourfold higher than EGCG. The higher antioxidant reactivity of **5c** can be explained by its structural features because *in silico* modeling predicted an intramolecular hydrogen bond with a bond length of 2.0 Å between the amino group and the hydroxy group of the molecule (Figure S10, Supporting Information). This hydrogen bond might stabilize the aroxyl radical of **5c** and facilitate the H-atom transfer to the DPPH radical resulting in a high biomolecular rate constant for **5c**.[43]

Inhibition of $A\beta_{42}$ fibrillation and effect on fibril disassembly. The amyloid cascade hypothesis is the predominant theory used to explain the pathophysiology of AD.[44] This hypothesis states that an imbalance between the production and clearance of Aβ in the brain[45] leads to amyloid deposition, which initiates a series of events, leading to synaptic dysfunction, neuronal loss, and neurotransmitter dysfunction.[46-48] The synthesized compounds were tested for their effect on the $A\beta_{42}$ fibrillation process. The amount of $A\beta_{42}$ protein fibrils in solution was measured using ProteoStat fluorescent dye which binds specifically to protein fibrils leading to an increase in the fluorescence intensity of the dye.[49] Compound **5c** significantly inhibited $A\beta_{42}$ fibrillation (Figure 2A), reducing the $A\beta_{42}$ fibril levels to 42.9% of $A\beta_{42}$ control. In comparison, EGCG showed a strong, almost complete inhibition of $A\beta_{42}$ fibrillation (3.78% of $A\beta_{42}$ control), and GA reduced the levels of fibrils to 15.4% of $A\beta_{42}$ control (Figure 2A).[40, 42, 50] The activity of **5c** was superior to that of the endogenous molecule KYNA which reduced the levels of fibrils to 68.0% of $A\beta_{42}$ control.

Moreover, **5c** was also tested for disassembly of preformed $A\beta_{42}$ fibrils in assays using dot-blot and ProteoStat dye. In the dot-blot assay, the destabilizing effect of **5c** on preformed $A\beta_{42}$ fibrils was clearly observed from day five onwards, using OC antibody which detects $A\beta_{42}$ fibrils[51] (Figure 2C). On day nine, very few fibrils were detected in the dot blot assay, which confirmed the destabilizing effect of **5c** on preformed $A\beta_{42}$ fibrils. Similarly, **5c** demonstrated a 41.5% reduction in total fibrils content in the ProteoStat disassembly assay (Figure 2B).

The effect of **5c** and reference compounds EGCG and GA on the morphology of $A\beta_{42}$ aggregates by the end of the fibrillation assay was studied by transmission electron microscopy (TEM) (Figure 2D). The $A\beta_{42}$ control showed a network of high-density fibrils while incubation of $A\beta_{42}$ with EGCG and GA resulted in amorphous structures.[40, 52] Similarly, incubation of $A\beta_{42}$ with **5c** resulted in low-density fibrils, thus confirming inhibition of $A\beta_{42}$ fibrillation by **5c**.

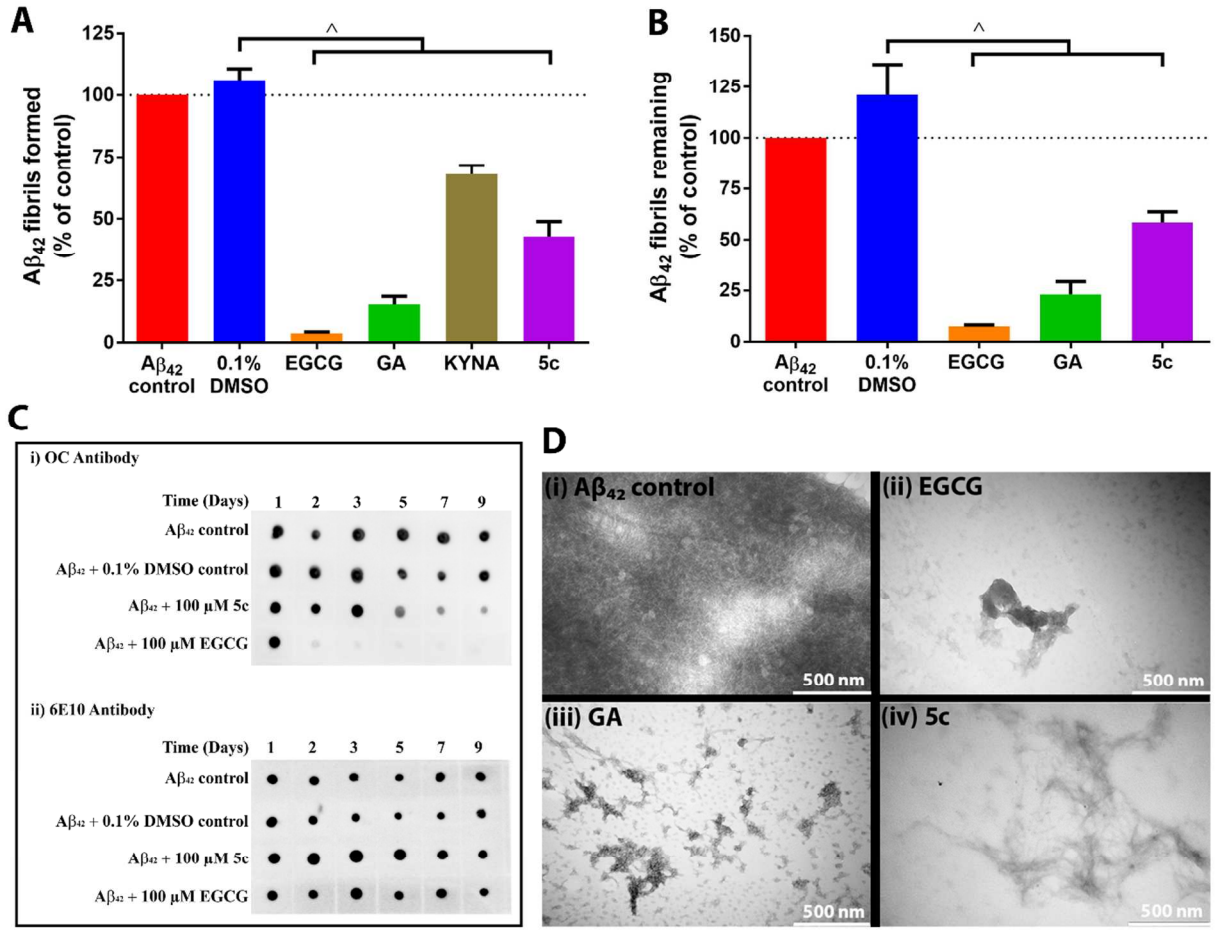

Figure 2. Effect of **5c** on $A\beta_{42}$ fibrillation and preformed $A\beta_{42}$ fibrils. (A) Extent of $A\beta_{42}$ fibrillation depicted as the percentage of the $A\beta_{42}$ control fluorescence intensity. $A\beta_{42}$ (27 μM) was incubated with 100 μM EGCG, GA, KYNA, or **5c** in phosphate buffer (20 mM, pH 7.4, *I* 0.17 M, DMSO 0.1% v/v) for 21 h at 37 °C under quiescent conditions. ProteoStat fluorescent dye was then added and fluorescence intensity was recorded (λ_{ex} 544 nm, λ_{em} 590 nm). Values are the mean ± SEM of four independent experiments. Statistical significance was determined by one-way ANOVA followed by Dunnett's multiple comparisons test with $^{\wedge}P < 0.0001$ c.f. to 0.1% DMSO control. (B) Disassembly of preformed $A\beta_{42}$ fibrils depicted as $A\beta_{42}$ fibrils remaining (% of the $A\beta_{42}$ control fluorescence intensity). $A\beta_{42}$ (27 μM) was incubated in phosphate buffer (20 mM, pH 7.4, *I* 0.17 M, DMSO 0.1% v/v) containing ProteoStat fluorescent dye, for 21 h at 37 °C under quiescent conditions. The fluorescence intensity was monitored (λ_{ex} 544 nm, λ_{em} 590 nm) to confirm fibril formation. The fibrils were then exposed to 100 μM EGCG, GA, or **5c** for 42 h at 37 °C under quiescent conditions and the fluorescence intensity was recorded (λ_{ex} 544 nm, λ_{em} 590 nm). Values are the mean ± SEM of three independent experiments. Statistical significance was determined by one-way ANOVA followed by Dunnett's multiple comparisons test with $^{\wedge}P < 0.0001$ c.f. to 0.1% DMSO control. (C) Dot-blot assay for determination of $A\beta_{42}$ fibril levels over 9 days in phosphate buffer (20 mM, pH 7.4, *I* 0.17 M) at 37 °C under quiescent conditions. $A\beta_{42}$ (27 μM) was incubated with 100 μM EGCG or **5c**. Compound **5c** contained DMSO (0.1% v/v). Sampling was conducted at various time points by spotting samples onto nitrocellulose membranes, and the membranes probed with either fibril-specific OC antibody[51] or 6E10 antibody[53] that recognizes all forms of Aβ *via* its residues 3-8. (D) Effect of EGCG, GA and **5c** on the morphology of $A\beta_{42}$ aggregates after 21 h of the fibrillation process. $A\beta_{42}$ (27 μM) was incubated with 100 μM EGCG, GA, or **5c**, in phosphate buffer (20 mM, pH 7.4, *I* 0.17 M, DMSO 0.1% v/v) at 37 °C under quiescent conditions. TEM images of: (i) $A\beta_{42}$ control; (ii) $A\beta_{42}$ + EGCG; (iii) $A\beta_{42}$ + GA; (iv) $A\beta_{42}$ + **5c**.

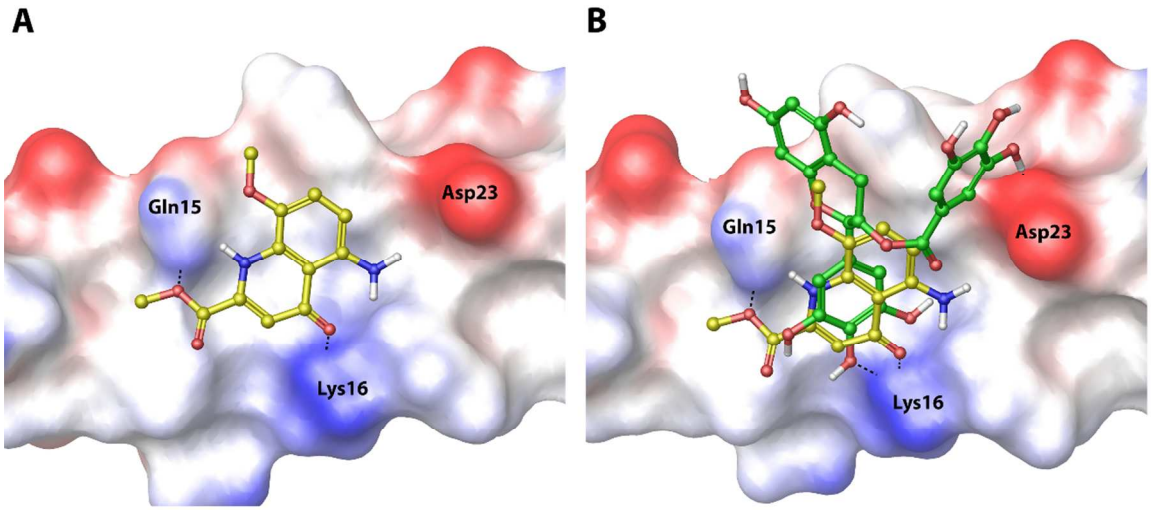

Figure 3. Docking models obtained from molecular modeling studies. (A) Docking model of **5c** with $A\beta_{42}$ peptide (PDB entry 1IYT) showing proposed binding orientation and interactions. $A\beta_{42}$ surface colors represents electrostatic potentials of residues (blue-positive, red-negative). (B) Superimposed docking pose of **5c** (yellow) and EGCG (green) with $A\beta_{42}$ peptide showing proposed binding interactions.

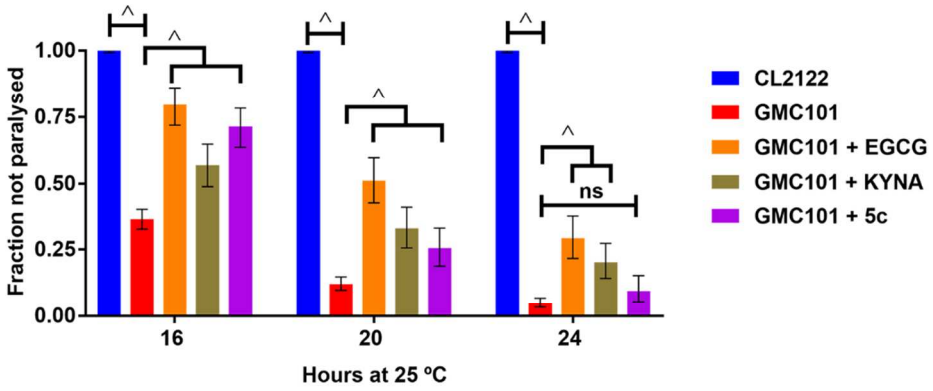

Figure 4. Protection against $A\beta_{42}$-induced toxicity in *C. elegans* at 25 °C. Plotted are the proportions of individuals not paralysed for untreated strains GMC101 and CL2122, and GMC101 grown in a Petri dish (30 mm x 15 mm) on media that was pre-treated with 100 µL of 2 mM of **5c**, KYNA and EGCG. Values are the mean with upper and lower 95% confidence intervals, based on data pooled from three independent experiments: Control strain CL2122 (n = 487),[50] $A\beta_{42}$ strain GMC101 (n = 678),[50] GMC101 strain + **5c** (n = 157), GMC101 strain + KYNA (n = 158), GMC101 strain + EGCG (n = 137),[50] where n = number of individuals assayed. Statistical significance was determined by a 5×2 Fisher's exact test, which gave an overall P value < 0.001. A series of 2×2 Fisher's exact tests were subsequently conducted for pairwise comparisons, applying the Bonferroni correction for multiple tests, with ^P < 0.007.

The ability of EGCG to inhibit Aβ fibril formation is believed to be due to interaction of EGCG and its quinone auto-oxidation products with hydrophobic binding sites in amyloid fibrils, and the formation of quinoprotein adducts by reaction of the quinones with Aβ lysine residues.[54, 55] The interactions of **5c** and EGCG[50] with $A\beta_{42}$ (PDB entry 1IYT[56]) were studied using molecular modeling (Figure 3A-B). This revealed similar predicted binding interactions, including proposed hydrogen bond interactions with the positively charged amino group of Lys16, and an additional proposed hydrogen bond between the ester oxygen atom of **5c** and the amino group of Gln15.

Protection against $A\beta_{42}$-induced toxicity in transgenic *C. elegans*. The effect of **5c**, KYNA and EGCG on Aβ-induced toxicity was studied *in vivo* using the transgenic GMC101 strain of *C. elegans*, which expresses full length $A\beta_{42}$ and develops severe, and fully penetrant, time-dependent paralysis at 25 °C (Figure 4).[25, 50] Strain CL2122, which does not express Aβ, was used as a transgenic control and exhibited no paralysis over the

time course of the experiment.[25, 50, 57] Previous studies showed that EGCG protects against Aβ-induced toxicity in transgenic *C. elegans* strains CL2006 and GMC101.[50, 58, 59] In this study, EGCG and KYNA showed a similar, statistically significant protective effect on the nematodes at all time points studied (16, 20 and 24 h), whereas compound **5c** displayed a statistically significant protective effect at the 16 and 20 h time points.

Blood-brain barrier permeability and inherent toxicity studies. BBB permeability is a critical parameter for CNS drugs and more than 98% of existing small molecule drugs do not cross the BBB.[60] BBB permeability was estimated by testing **3b**, **5b, 5c**, EGCG and GA in a bi-directional permeability assay using an MDR1-MDCKII cell monolayer (Table 3).[61, 62] Fenoterol and propranolol were used as low and high permeability markers, respectively, and digoxin was used as a P-glycoprotein substrate. EGCG, GA, and **3b** had low permeability across the cell monolayer, whereas **5b** and **5c** had high permeability with mean P_{app} values of 31.4×10^{-6} cm/s and 28.7×10^{-6} cm/s, respectively. Both **5b** and **5c** presented a low efflux ratio, which indicates that these compounds do not belong to the P-glycoprotein substrate category. Compound **3b** had poor recovery from the assay, and there is potential for hydrolysis of the methyl ester to the free acid, which could be a reason for its low permeability. On the other hand, the low permeability of EGCG and GA may be attributed to their poor drug-likeness.[40] All synthesized analogs of KYNA were tested for inherent toxicity using SH-SY5Y neuroblastoma cells in an MTT cell viability assay. Except for **4a**, none of the compounds were found to have any significant toxicity up to 100 μM over a period of 48 h (Supporting Information).

Table 3. Permeability across an MDR1-MDCKII cell monolayer.[a]

Compound	Mean P_{app} (10^{-6} cm/s)	Efflux ratio[b]	Mean recovery (%)	BBB category[c]
Fenoterol	0.22	-	90.3	Low
Propranolol	21.1	-	70.8	High
Digoxin	0.10	78.5	65.3	Low
3b	0.31	0.02	0.78	Low
5b	28.7	0.66	86.7	High
5c	31.4	0.63	76.1	High
EGCG	0.07	2.97	62.9	Low
Gallic acid	0.01	29.3	65.0	Low

[a]Test concentration 2 μM; incubation time 2.5 h. [b](P_{app} B to A) / (P_{app} A to B). [c]Binning Criteria: Low permeability: $P_{app} \leq 1.0$ ($\times 10^{-6}$ cm/s); Moderate permeability: $1.0 < P_{app} < 5.5$ ($\times 10^{-6}$ cm/s); High permeability: $P_{app} \geq 5.5$ ($\times 10^{-6}$ cm/s); The boundaries for low and high permeability binning are equivalent to 50% and 80% of the "calculated Fa" in human.

CONCLUSIONS

Chemical modifications of endogenous molecules can lead to the development of new analogs with improved potency and drug-like properties. These modifications could also be useful for the development of compounds with multifunctional properties. By utilizing this approach, here we reported the synthesis and evaluation of multifunctional analogs of KYNA for the treatment of AD. All of the synthesized compounds were tested for their NMDAR binding, mGluR5 binding and function, AChE inhibition, free radical scavenging ability and effect on $A\beta_{42}$ fibril formation and disassembly, which are mechanisms by which drugs can target AD. Of note was compound **5c**, which displayed activity through multiple target mechanisms with disease-modifying potential. In particular, **5c** had a high stoichiometric bimolecular rate constant for free radical scavenging which was superior to that of the potent antioxidant EGCG. In the $A\beta_{42}$ fibrillation process, **5c** exhibited 57.1% reduction in $A\beta_{42}$ control amplitude and TEM images showed very low density fibrils with some amorphous structures. Compound **5c** also showed a significant disassembly of preformed $A\beta_{42}$ fibrils in dot-blot and ProteoStat dye fibril disassembly assays. Interestingly, **5c** protected a transgenic *C. elegans* strain from $A\beta_{42}$-induced toxicity in a similar manner to EGCG and KYNA. Compound **5b** was also interesting, because it had moderate potency in the DPPH radical scavenging process, which is a prospective disease modifying property, and it showed 42.4% inhibition in the NMDAR binding assay with a K_i value of 7.98 μM. Compound **5b** also had a K_i value 0.829 μM for mGluR5 binding. One of the promising features of **5b** and **5c** is their predicted high BBB permeability. Both of these compounds displayed high permeability across an MDR1-MDCKII cell monolayer model of the BBB, even higher than that of the high permeability reference drug propranolol, and more than 400-fold better than the reference antioxidant/anti-Aβ compounds EGCG and GA, which displayed very low permeability. Compound **3b** emerged with specific activity as a micromolar AChE inhibitor (*Ee*AChE IC_{50} 10.9 μM), however it had low permeability in the BBB model. None of **3b**, **5b** and **5c** were toxic to SH-SY5Y neuronal cells up to 100 μM over a period of 48 h. Both **5b** and **5c** provide opportunities for future development of multifunctional molecules based on this scaffold. This study highlights how modification of endogenous molecules is a useful strategy for the development of novel therapeutic agents.

ASSOCIATED CONTENT

Supporting Information.

The Supporting Information is available free of charge on the ACS Publications website at DOI: 10.1021/acschemneuro.XXX

General materials and methods, synthetic procedures along with ^{1}H NMR, ^{13}C NMR and MS data, procedures for computational studies, experimental procedures for pharmacological evaluation (AChE inhibition assay, DPPH

assay, ProteoStat assay, TEM, dot-blot assay, paralysis assay using transgenic *C. elegans*, estimation of BBB permeability using MDR1-MDCKII cells, inherent toxicity using SH-SY5Y cells), additional docking images, AChE concentration-response curves for **3a**, **3b**, **4b**, and rivastigmine, representative absorbance-time plots of the bleaching of DPPH by **5a**, **5b** and **5c**, *in silico* prediction of intramolecular hydrogen bonding in **5c**, graphs showing inherent toxicity towards SH-SY5Y cells**.**

AUTHOR INFORMATION

Corresponding Author

*Tel: +61 7 33461900. Fax: +61 7 33461999. Email: b.ross1@uq.edu.au.

Author Contributions

G.S.D. and B.P.R. designed the study. G.S.D. carried out synthesis of compounds, biological assays and molecular docking studies. S.K. contributed to the paralysis studies in *C. elegans* and dot-blot assay. S.C. contributed to the toxicity studies, paralysis studies in *C. elegans* and acquired the TEM images. G.M. contributed to the paralysis studies in *C. elegans*. S.N.D. contributed to the cholinesterase inhibition assay and ProteoStat assay. S.K.V. contributed to the ProteoStat assay. M.O.P. contributed to the dot blot assay and toxicity studies. R.P.M contributed to the synthesis of compounds. G.S.D. and B.P.R. wrote the manuscript. All authors read and approved the final manuscript.

Funding Sources

Funding for this work was provided by The University of Queensland. G.S.D., S.K., S.C., S.N.D., and S.K.V. thank UQ for PhD scholarships.

Notes

The authors declare no competing financial interest.

ACKNOWLEDGMENTS

K_i determinations, receptor binding profiles, agonist and antagonist functional data for NMDAR and mGluR5, was generously provided by the National Institute of Mental Health's Psychoactive Drug Screening Program, Contract # HHSN-271-2013-00017-C (NIMH PDSP). The NIMH PDSP is Directed by Bryan L. Roth MD, PhD at the University of North Carolina at Chapel Hill and Project Officer Jamie Driscoll at NIMH, Bethesda MD, USA. Some *C. elegans* strains were provided by the Caenorhabditis Genetics Center (CGC), supported by the US National Institutes of Health-Office of Research Infrastructure Programs (P40 OD010440). The authors acknowledge the facilities, and the scientific and technical assistance, of the Australian Microscopy & Microanalysis Research Facility at the Centre for Microscopy and Microanalysis, UQ. G.S.D. and B.P.R. thank Prof Nick Shaw and Dr Peter Moyle, UQ, for helpful discussions.

ABBREVIATIONS

Aβ, amyloid beta peptide; AD, Alzheimer's disease; AChE, acetylcholinesterase; BBB, blood-brain barrier; CNS, central nervous system; *Ee*AChE, acetylcholinesterase from *Electrophorus electricus*; EGCG, (−)-epigallocatechin gallate; GA, gallic acid; KYNA, kynurenic acid; mGlur5, metabotropic glutamate receptor 5; MPEP, 2-methyl-6-(phenylethynyl)pyridine; NMDA, *N*-methyl-D-aspartate; PPA, polyphosphoric acid; TEM, transmission electron microscopy.

REFERENCES

(1) Gonda, X. (2012) Basic pharmacology of NMDA receptors, *Curr. Pharm. Des. 18*, 1558-1567.

(2) Ghasemi, M., and Schachter, S. C. (2011) The NMDA receptor complex as a therapeutic target in epilepsy: a review, *Epilepsy Behav. 22*, 617-640.

(3) Malinow, R. (2012) New developments on the role of NMDA receptors in Alzheimer's disease, *Curr. Opin. Neurobiol. 22*, 559-563.

(4) Mota, S. I., Ferreira, I. L., and Rego, A. C. (2014) Dysfunctional synapse in Alzheimer's disease - A focus on NMDA receptors, *Neuropharmacology 76 Pt A*, 16-26.

(5) Mayeux, R., and Stern, Y. (2012) Epidemiology of Alzheimer Disease, *Cold Spring Harb. Perspect. Med. 2*, 10.1101/cshperspect.a006239 a006239.

(6) Heidelberger, C., Gullberg, M. E., and et al. (1949) Tryptophan metabolism; concerning the mechanism of the mammalian conversion of tryptophan into kynurenine, kynurenic acid, and nicotinic acid, *J. Biol. Chem. 179*, 143-150.

(7) Birch, P. J., Grossman, C. J., and Hayes, A. G. (1988) Kynurenic acid antagonises responses to NMDA via an action at the strychnine-insensitive glycine receptor, *Eur. J. Pharmacol. 154*, 85-87.

(8) Schwarcz, R., Bruno, J. P., Muchowski, P. J., and Wu, H. Q. (2012) Kynurenines in the mammalian brain: when physiology meets pathology, *Nat. Rev. Neurosci. 13*, 465-477.

(9) Schwarcz, R., Bruno, J. P., Muchowski, P. J., and Wu, H. Q. (2012) Kynurenines in the mammalian brain: when physiology meets pathology, *Nat. Rev. Neurosci. 13*, 465-477.

(10) Baron, B. M., Harrison, B. L., Miller, F. P., McDonald, I. A., Salituro, F. G., Schmidt, C. J., Sorensen, S. M., White, H. S., and Palfreyman, M. G. (1990) Activity of 5,7-dichlorokynurenic acid, a potent antagonist at the N-methyl-D-aspartate receptor-associated glycine binding site, *Mol. Pharmacol. 38*, 554-561.

(11) Yiannopoulou, K. G., and Papageorgiou, S. G. (2013) Current and future treatments for Alzheimer's disease, *Ther. Adv. Neurol. Disord. 6*, 19-33.

(12) Takeda, A., Loveman, E., Clegg, A., Kirby, J., Picot, J., Payne, E., and Green, C. (2006) A systematic review of the clinical effectiveness of donepezil, rivastigmine and galantamine on cognition, quality of life and adverse events in Alzheimer's disease, *Int. J. Geriatr. Psychiatry 21*, 17-28.

(13) Johnson, J. W., Glasgow, N. G., and Povysheva, N. V. (2015) Recent insights into the mode of action of memantine and ketamine, *Curr. Opin. Pharm. 0*, 54-63.

(14) Iqbal, K., and Grundke-Iqbal, I. (2010) Alzheimer's disease, a multifactorial disorder seeking multitherapies, *Alzheimers Dement. 6*, 420-424.

(15) Wang, L., Esteban, G., Ojima, M., Bautista-Aguilera, O. M., Inokuchi, T., Moraleda, I., Iriepa, I., Samadi, A., Youdim, M. B., Romero, A., Soriano, E., Herrero, R.,

Fernandez Fernandez, A. P., Ricardo Martinez, M., Marco-Contelles, J., and Unzeta, M. (2014) Donepezil + propargylamine + 8-hydroxyquinoline hybrids as new multifunctional metal-chelators, ChE and MAO inhibitors for the potential treatment of Alzheimer's disease, *Eur. J. Med. Chem. 80*, 543-561.

(16) Mao, F., Yan, J., Li, J., Jia, X., Miao, H., Sun, Y., Huang, L., and Li, X. (2014) New multi-target-directed small molecules against Alzheimer's disease: a combination of resveratrol and clioquinol, *Org. Biomol. Chem. 12*, 5936-5944.

(17) Bag, S., Tulsan, R., Sood, A., Cho, H., Redjeb, H., Zhou, W., LeVine, H., 3rd, Torok, B., and Torok, M. (2015) Sulfonamides as multifunctional agents for Alzheimer's disease, *Bioorg. Med. Chem. Lett. 25*, 626-630.

(18) Fernandez-Bachiller, M. I., Perez, C., Monjas, L., Rademann, J., and Rodriguez-Franco, M. I. (2012) New tacrine-4-oxo-4H-chromene hybrids as multifunctional agents for the treatment of Alzheimer's disease, with cholinergic, antioxidant, and beta-amyloid-reducing properties, *J. Med. Chem. 55*, 1303-1317.

(19) Guzior, N., Wieckowska, A., Panek, D., and Malawska, B. (2015) Recent development of multifunctional agents as potential drug candidates for the treatment of Alzheimer's disease, *Curr. Med. Chem. 22*, 373-404.

(20) Kumar, A., Dhull, D. K., and Mishra, P. S. (2015) Therapeutic potential of mGluR5 targeting in Alzheimer's disease, *Front. Neurosci. 9*, 215.

(21) Abushik, P. A., Niittykoski, M., Giniatullina, R., Shakirzyanova, A., Bart, G., Fayuk, D., Sibarov, D. A., Antonov, S. M., and Giniatullin, R. (2014) The role of NMDA and mGluR5 receptors in calcium mobilization and neurotoxicity of homocysteine in trigeminal and cortical neurons and glial cells, *J. Neurochem. 129*, 264-274.

(22) Hamilton, A., Vasefi, M., Vander Tuin, C., McQuaid, R. J., Anisman, H., and Ferguson, S. S. (2016) Chronic Pharmacological mGluR5 Inhibition Prevents Cognitive Impairment and Reduces Pathogenesis in an Alzheimer Disease Mouse Model, *Cell Rep 15*, 1859-1865.

(23) O'Leary, D. M., Movsesyan, V., Vicini, S., and Faden, A. I. (2000) Selective mGluR5 antagonists MPEP and SIB-1893 decrease NMDA or glutamate-mediated neuronal toxicity through actions that reflect NMDA receptor antagonism, *Br. J. Pharmacol. 131*, 1429-1437.

(24) Byrnes, K. R., Loane, D. J., Stoica, B. A., Zhang, J., and Faden, A. I. (2012) Delayed mGluR5 activation limits neuroinflammation and neurodegeneration after traumatic brain injury, *J. Neuroinflammation 9*, 43.

(25) McColl, G., Roberts, B. R., Pukala, T. L., Kenche, V. B., Roberts, C. M., Link, C. D., Ryan, T. M., Masters, C. L., Barnham, K. J., Bush, A. I., and Cherny, R. A. (2012) Utility of an improved model of amyloid-beta (Aβ1-42) toxicity in Caenorhabditis elegansfor drug screening for Alzheimer's disease, *Mol. Neurodegener. 7*, 57.

(26) Heindel, N. D., Bechara, I. S., Kennewell, P. D., Molnar, J., Ohnmacht, C. J., Lemke, S. M., and Lemke, T. F. (1968) Cyclization of aniline-acetylenedicarboxylate adducts. A modified Conrad-Limpach method for the synthesis of potential antimalarials, *J. Med. Chem. 11*, 1218-1221.

(27) Mazzoni, O., Esposito, G., Diurno, M. V., Brancaccio, D., Carotenuto, A., Grieco, P., Novellino, E., and Filippelli, W. (2010) Synthesis and Pharmacological Evaluation of Some 4-Oxo-quinoline-2-carboxylic Acid Derivatives as Anti-inflammatory and Analgesic Agents, *Arch. Pharm. 343*, 561-569.

(28) Peet, N. P., Baugh, L. E., Sunder, S., and Lewis, J. E. (1985) Synthesis and antiallergic activity of some quinolinones and imidazoquinolinones, *J. Med. Chem. 28*, 298-302.

(29) Ferlin, M. G., Chiarelotto, G., and Castagliuolo, I. (2002) Synthesis and characterization of some N-mannich bases of [1,2,3]triazoloquinolines, *J. Heterocycl. Chem. 39*, 631-638.

(30) Hu, Y., Lin, E. C., Pham, L. M., Cajica, J., Amantea, C. M., Okerberg, E., Brown, H. E., Fraser, A., Du, L., Kohno, Y., Ishiyama, J., Kozarich, J. W., and Shreder, K. R. (2013) Amides of 4-hydroxy-8-methanesulfonylamino-quinoline-2-carboxylic acid as zinc-dependent inhibitors of Lp-PLA(2), *Bioorg. Med. Chem. Lett. 23*, 1553-1556.

(31) Roth, B. L. (2013) National Institute of Mental Health Psychoactive Drug Screening Program (NIMH PDSP), Assay protocol book, Version II, Department of Pharmacology, University of North Carolina at Chapel Hill, Chapel Hill, NC 27599.

(32) Besnard, J., Ruda, G. F., Setola, V., Abecassis, K., Rodriguiz, R. M., Huang, X.-P., Norval, S., Sassano, M. F., Shin, A. I., Webster, L. A., Simeons, F. R. C., Stojanovski, L., Prat, A., Seidah, N. G., Constam, D. B., Bickerton, G. R., Read, K. D., Wetsel, W. C., Gilbert, I. H., Roth, B. L., and Hopkins, A. L. (2012) Automated design of ligands to polypharmacological profiles, *Nature 492*, 10.1038/nature11691.

(33) Dighe, S. N., Deora, G. S., De la Mora, E., Nachon, F., Chan, S., Parat, M. O., Brazzolotto, X., and Ross, B. P. (2016) Discovery and Structure-Activity Relationships of a Highly Selective Butyrylcholinesterase Inhibitor by Structure-Based Virtual Screening, *J. Med. Chem. 59*, 7683-7689.

(34) Furukawa, H., and Gouaux, E. (2003) Mechanisms of activation, inhibition and specificity: crystal structures of the NMDA receptor NR1 ligand-binding core, *EMBO J. 22*, 2873-2885.

(35) Dore, A. S., Okrasa, K., Patel, J. C., Serrano-Vega, M., Bennett, K., Cooke, R. M., Errey, J. C., Jazayeri, A., Khan, S., Tehan, B., Weir, M., Wiggin, G. R., and Marshall, F. H. (2014) Structure of class C GPCR metabotropic glutamate receptor 5 transmembrane domain, *Nature 511*, 557-562.

(36) Ellman, G. L., Courtney, K. D., Andres, V., and Featherstone, R. M. (1961) A new and rapid colorimetric determination of acetylcholinesterase activity, *Biochem. Pharmacol. 7*, 88-95.

(37) Saxena, A., Redman, A. M., Jiang, X., Lockridge, O., and Doctor, B. P. (1997) Differences in active site gorge dimensions of cholinesterases revealed by binding of inhibitors to human butyrylcholinesterase, *Biochemistry 36*, 14642-14651.

(38) Kryger, G., Silman, I., and Sussman, J. L. (1999) Structure of acetylcholinesterase complexed with E2020 (Aricept): implications for the design of new anti-Alzheimer drugs, *Structure 7*, 297-307.

(39) Blois, M. S. (1958) Antioxidant Determinations by the Use of a Stable Free Radical, *Nature 181*, 1199-1200.

(40) Chan, S., Kantham, S., Rao, V. M., Palanivelu, M. K., Pham, H. L., Shaw, P. N., McGeary, R. P., and Ross, B. P. (2016) Metal chelation, radical scavenging and

inhibition of Abeta42 fibrillation by food constituents in relation to Alzheimer's disease, *Food Chem. 199*, 185-194.
(41) Shi, H., and Niki, E. (1998) Stoichiometric and kinetic studies on Ginkgo biloba extract and related antioxidants, *Lipids 33*, 365-370.
(42) Bastianetto, S., Yao, Z. X., Papadopoulos, V., and Quirion, R. (2006) Neuroprotective effects of green and black teas and their catechin gallate esters against beta-amyloid-induced toxicity, *Eur. J. Neurosci. 23*, 55-64.
(43) Amorati, R., Lucarini, M., Mugnaini, V., and Pedulli, G. F. (2003) Antioxidant activity of o-bisphenols: the role of intramolecular hydrogen bonding, *J. Org. Chem. 68*, 5198-5204.
(44) Pangalos, M. N., Jacobsen, S. J., and Reinhart, P. H. (2005) Disease modifying strategies for the treatment of Alzheimer's disease targeted at modulating levels of the β-amyloid peptide, *Biochem. Soc. Trans. 33*, 553-558.
(45) Blennow, K., de Leon, M. J., and Zetterberg, H. Alzheimer's disease, *Lancet 368*, 387-403.
(46) Karran, E., Mercken, M., and De Strooper, B. (2011) The amyloid cascade hypothesis for Alzheimer's disease: an appraisal for the development of therapeutics, *Nat. Rev. Drug Discov. 10*, 698-U1600.
(47) Tayeb, H. O., Murray, E. D., Price, B. H., and Tarazi, F. I. (2013) Bapineuzumab and solanezumab for Alzheimer's disease: is the 'amyloid cascade hypothesis' still alive?, *Expert Opin. Biol. Ther. 13*, 1075-1084.
(48) Gandy, S., Martins, R. N., and Buxbaum, J. (2003) Molecular and cellular basis for anti-amyloid therapy in Alzheimer disease, *Alzheimer Dis. Assoc. Disord. 17*, 259-266.
(49) Navarro, S., and Ventura, S. (2014) Fluorescent dye ProteoStat to detect and discriminate intracellular amyloid-like aggregates in Escherichia coli, *Biotechnol. J. 9*, 1259-1266.
(50) Kantham, S., Chan, S., McColl, G., Miles, J. A., Veliyath, S. K., Deora, G. S., Dighe, S. N., Khabbazi, S., Parat, M. O., and Ross, B. P. (2017) Effect of the Biphenyl Neolignan Honokiol on Abeta42-Induced Toxicity in Caenorhabditis elegans, Abeta42 Fibrillation, Cholinesterase Activity, DPPH Radicals, and Iron(II) Chelation, *ACS Chem. Neurosci. DOI.10.1021/acschemneuro.7b00071*.
(51) Kayed, R., Head, E., Sarsoza, F., Saing, T., Cotman, C. W., Necula, M., Margol, L., Wu, J., Breydo, L., Thompson, J. L., Rasool, S., Gurlo, T., Butler, P., and Glabe, C. G. (2007) Fibril specific, conformation dependent antibodies recognize a generic epitope common to amyloid fibrils and fibrillar oligomers that is absent in prefibrillar oligomers, *Mol. Neurodegener. 2*, 18.
(52) Ehrnhoefer, D. E., Bieschke, J., Boeddrich, A., Herbst, M., Masino, L., Lurz, R., Engemann, S., Pastore, A., and Wanker, E. E. (2008) EGCG redirects amyloidogenic polypeptides into unstructured, off-pathway oligomers, *Nat. Struct. Mol. Biol. 15*, 558-566.
(53) Klyubin, I., Walsh, D. M., Lemere, C. A., Cullen, W. K., Shankar, G. M., Betts, V., Spooner, E. T., Jiang, L., Anwyl, R., Selkoe, D. J., and Rowan, M. J. (2005) Amyloid beta protein immunotherapy neutralizes Abeta oligomers that disrupt synaptic plasticity in vivo, *Nat. Med. 11*, 556-561.
(54) Sato, M., Murakami, K., Uno, M., Nakagawa, Y., Katayama, S., Akagi, K., Masuda, Y., Takegoshi, K., and Irie, K. (2013) Site-specific inhibitory mechanism for amyloid beta42 aggregation by catechol-type flavonoids targeting the Lys residues, *J. Biol. Chem. 288*, 23212-23224.
(55) Palhano, F. L., Lee, J., Grimster, N. P., and Kelly, J. W. (2013) Toward the molecular mechanism(s) by which EGCG treatment remodels mature amyloid fibrils, *J. Am. Chem. Soc. 135*, 7503-7510.
(56) Crescenzi, O., Tomaselli, S., Guerrini, R., Salvadori, S., D'Ursi, A. M., Temussi, P. A., and Picone, D. (2002) Solution structure of the Alzheimer amyloid beta-peptide (1-42) in an apolar microenvironment. Similarity with a virus fusion domain, *Eur. J. Biochem. 269*, 5642-5648.
(57) Fay, D. S., Fluet, A., Johnson, C. J., and Link, C. D. (1998) In vivo aggregation of beta-amyloid peptide variants, *J. Neurochem. 71*, 1616-1625.
(58) Abbas, S., and Wink, M. (2010) Epigallocatechin gallate inhibits beta amyloid oligomerization in Caenorhabditis elegans and affects the daf-2/insulin-like signaling pathway, *Phytomedicine 17*, 902-909.
(59) Zhang, L., Jie, G., Zhang, J., and Zhao, B. (2009) Significant longevity-extending effects of EGCG on Caenorhabditis elegans under stress, *Free Radic. Biol. Med. 46*, 414-421.
(60) Pardridge, W. M. (2005) The Blood-Brain Barrier: Bottleneck in Brain Drug Development, *NeuroRx 2*, 3-14.
(61) Bakos, E., Evers, R., Szakacs, G., Tusnady, G. E., Welker, E., Szabo, K., de Haas, M., van Deemter, L., Borst, P., Varadi, A., and Sarkadi, B. (1998) Functional multidrug resistance protein (MRP1) lacking the N-terminal transmembrane domain, *J. Biol. Chem. 273*, 32167-32175.
(62) Di, L., Kerns, E. H., and Carter, G. T. (2008) Strategies to assess blood-brain barrier penetration, *Expert opinion on drug discovery 3*, 677-687.

Table of Contents Graphic

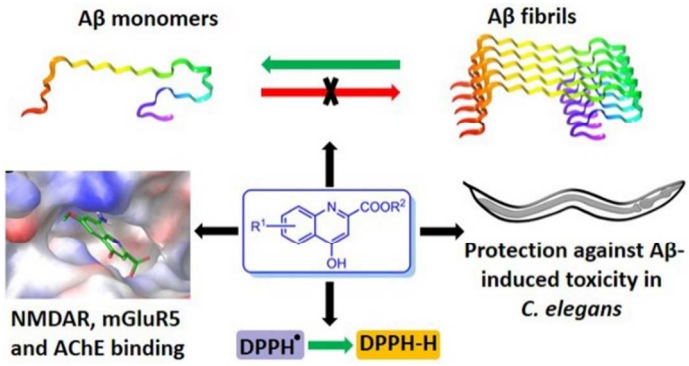

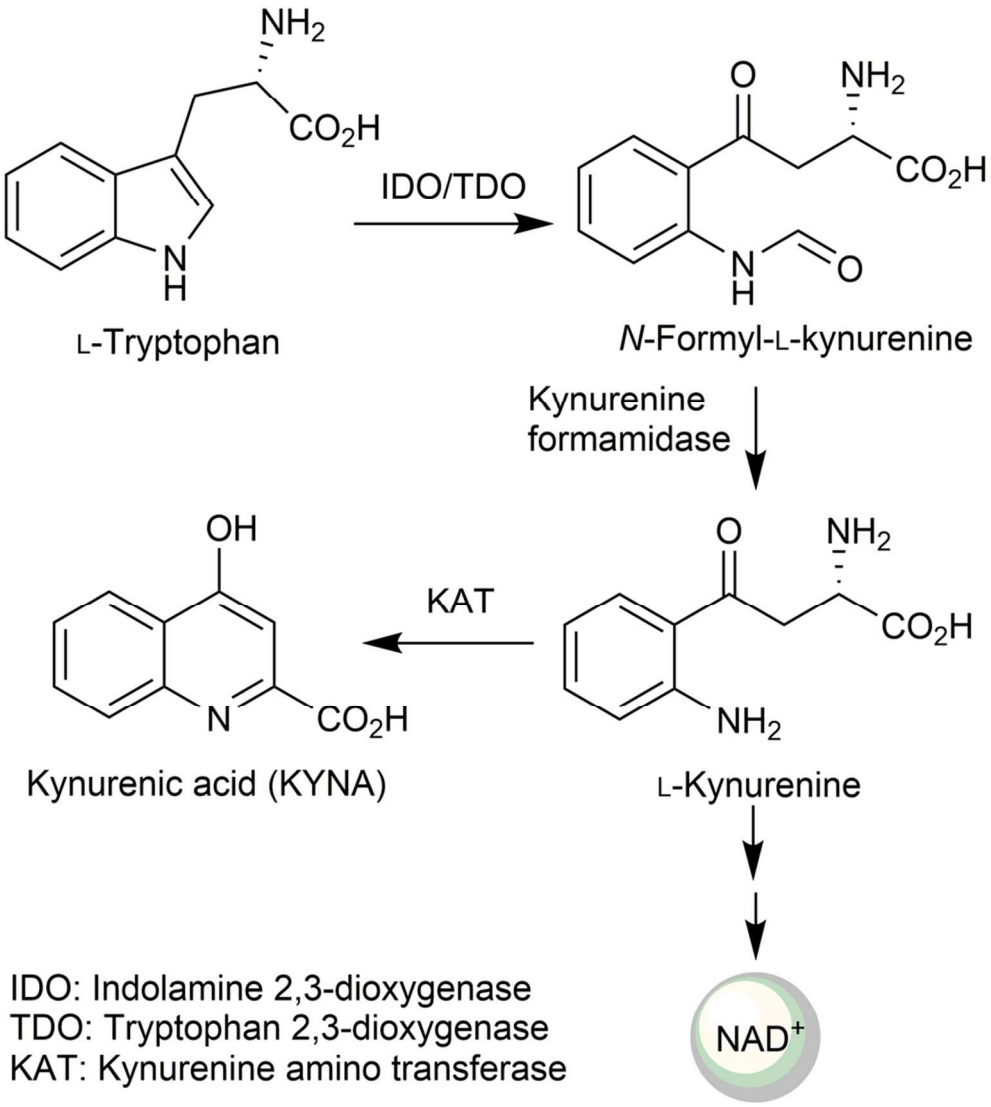

Scheme 1. Biosynthesis of kynurenic acid via tryptophan metabolism.

89x99mm (300 x 300 DPI)

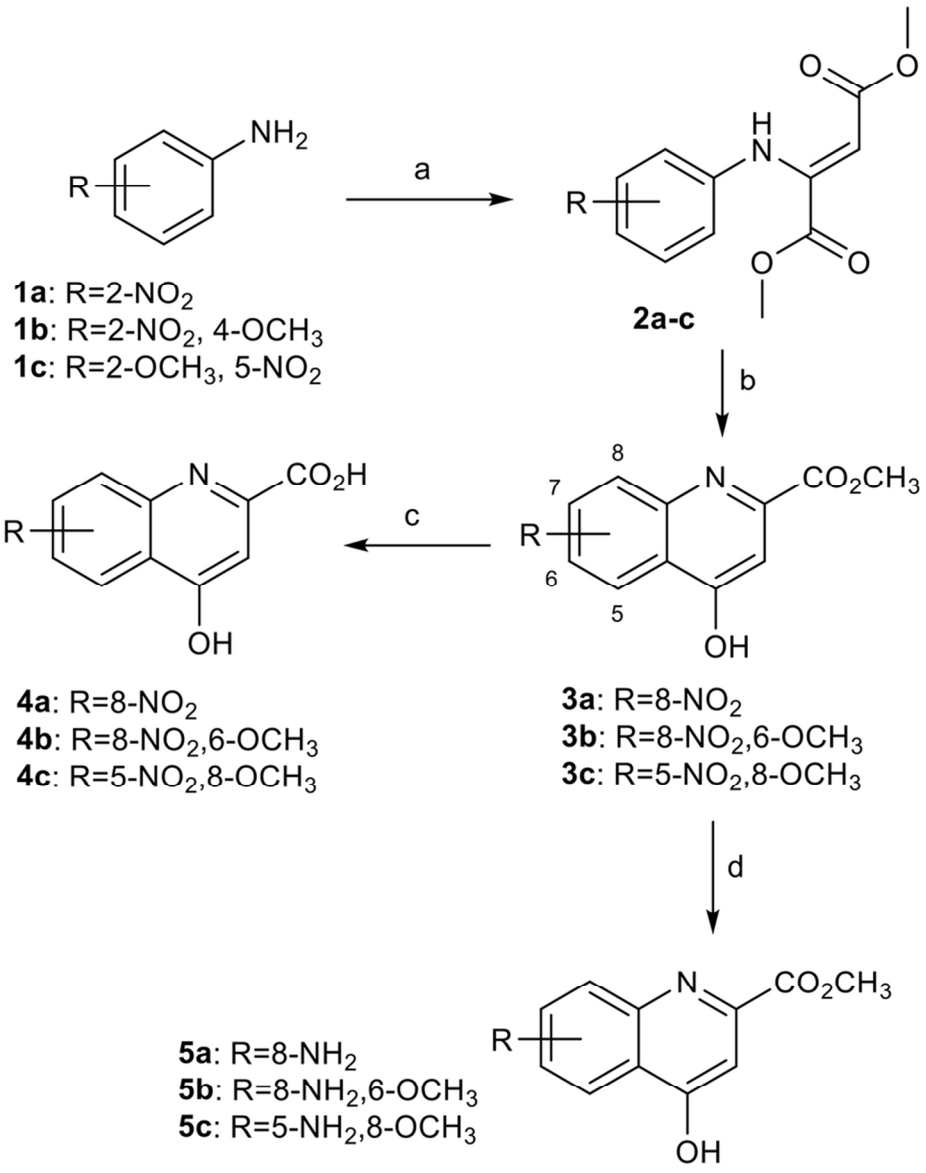

Scheme 2. Synthesis of analogs of kynurenic acid.a
aReagents and conditions: (a) Dimethyl acetylenedicarbox-ylate, CH3OH, reflux, 3-5 h (64-87%); (b) PPA, 120 oC, 1 h (28-65%); (c) CH3OH, 2 M aq. NaOH, r.t., 0.5-1 h (83-90%); (d) 5% Pd/C, H2, CH3OH, r.t., 4 h (40-95%).

88x106mm (300 x 300 DPI)

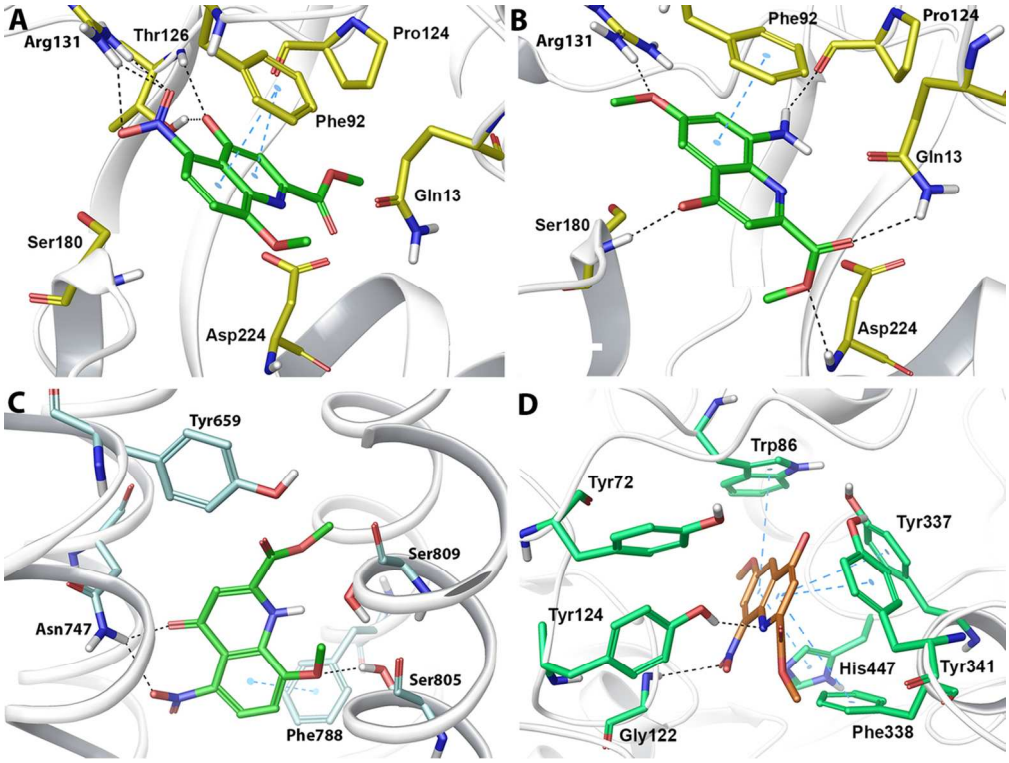

Figure 1. Docking models obtained from molecular modeling studies. (A,B) Proposed binding interactions of 3c (A) and 5b (B) with active site residues of the glycine-binding site of the NMDAR (PDB entry: 1PBQ). Binding site residues are depicted as sticks with carbon atoms represented in yellow (green for 3c and 5b). (C) Docked model of a tautomer of 3c with mGluR5 (PDB entry: 4OO9) showing proposed binding interactions. Protein residues are represented as sticks with carbon atoms in turquoise (green for 3c). (D) Docked model of 3b with huAChE (PDB entry: 4EY7) showing proposed binding interactions with the active site pocket. Active site residues are represented as sticks with carbon atoms in green (orange for 3b) The black dashed lines repre-sent hydrogen bonds, and light blue dashed lines represent π-π stacking. In all figures, the black dashed lines represent hydro-gen bonds, and light blue dashed lines represent π-π stacking between ligand and receptor.

114x86mm (300 x 300 DPI)

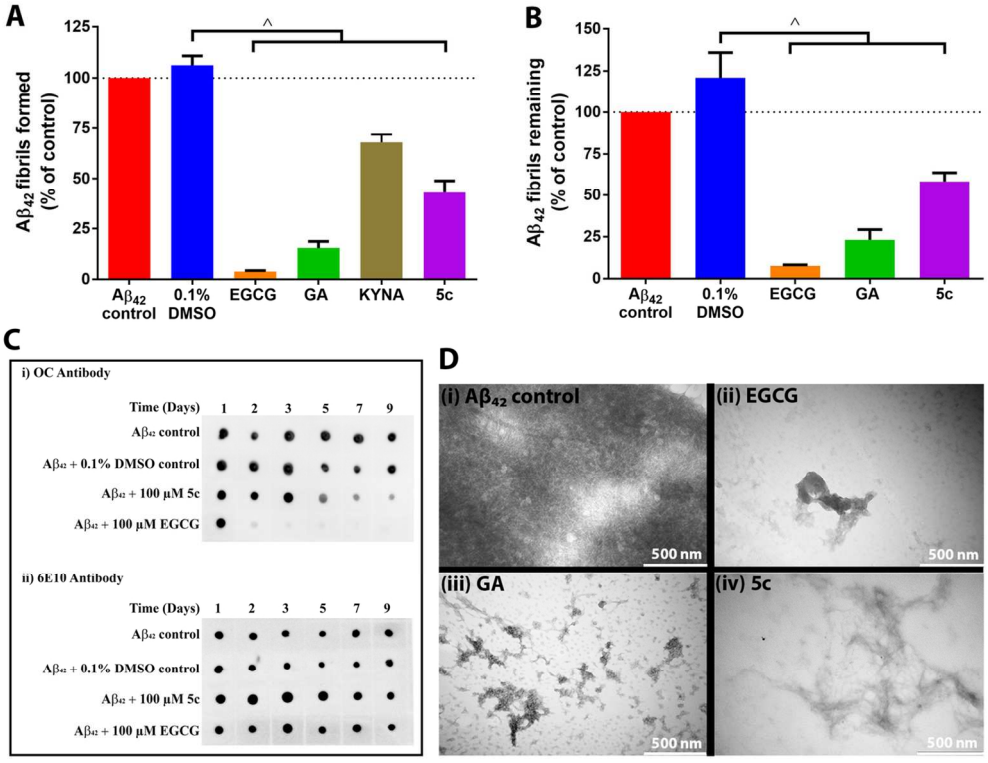

Figure 2. Effect of 5c on Aβ42 fibrillation and preformed Aβ42 fibrils. (A) Extent of Aβ42 fibrillation depicted as the percentage of the Aβ42 control fluorescence intensity. Aβ42 (27 μM) was incubated with 100 μM EGCG, GA, KYNA, or 5c in phosphate buffer (20 mM, pH 7.4, I 0.17 M, DMSO 0.1% v/v) for 21 h at 37 oC under quiescent conditions. ProteoStat fluorescent dye was then added and fluorescence intensity was recorded (λex 544 nm, λem 590 nm). Values are the mean ± SEM of four independent experiments. Statistical significance was determined by one-way ANOVA followed by Dunnett's multiple comparisons test with ^P < 0.0001 c.f. to 0.1% DMSO control. (B) Disassembly of preformed Aβ42 fibrils depicted as Aβ42 fibrils remaining (% of the Aβ42 control fluo-rescence intensity). Aβ42 (27 μM) was incubated in phosphate buffer (20 mM, pH 7.4, I 0.17 M, DMSO 0.1% v/v) containing Pro-teoStat fluorescent dye, for 21 h at 37 °C under quiescent conditions. The fluorescence intensity was monitored (λex 544 nm, λem 590 nm) to confirm fibril formation. The fibrils were then exposed to 100 μM EGCG, GA, or 5c for 42 h at 37 oC under quiescent conditions and the fluorescence intensity was recorded (λex 544 nm, λem 590 nm). Values are the mean ± SEM of three independ-ent experiments. Statistical significance was determined by one-way ANOVA followed by Dunnett's multiple comparisons test with ^P < 0.0001 c.f. to 0.1% DMSO control. (C) Dot-blot assay for determination of Aβ42 fibril levels over 9 days in phosphate buffer (20 mM, pH 7.4, I 0.17 M) at 37 oC under quiescent conditions. Aβ42 (27 μM) was incubated with 100 μM EGCG or 5c. Compound 5c contained DMSO (0.1% v/v). Sampling was conducted at various time points by spotting samples onto nitrocellu-lose membranes, and the membranes probed with either fibril-specific OC antibody51 or 6E10 antibody53 that recognizes all forms of Aβ via its residues 3-8. (D) Effect of EGCG, GA and 5c on the morphology of Aβ42 aggregates after 21 h of the fibrillation process. Aβ42 (27 μM) was incubated with 100 μM EGCG, GA, or 5c, in phosphate buffer (20 mM, pH 7.4, I 0.17 M, DMSO 0.1% v/v) at 37 °C under quiescent conditions. TEM images of: (i) Aβ42 control; (ii) Aβ42 + EGCG; (iii) Aβ42 + GA; (iv) Aβ42 + 5c.

124x96mm (300 x 300 DPI)

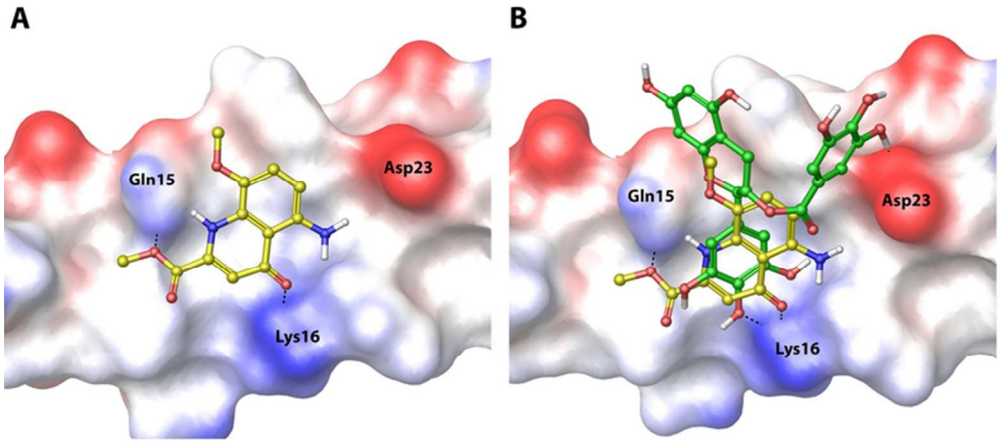

Figure 3. Docking models obtained from molecular modeling studies. (A) Docking model of 5c with Aβ42 peptide (PDB entry 1IYT) showing proposed binding orientation and interactions. Aβ42 surface colors represents electrostatic potentials of residues (blue-positive, red-negative). (B) Superimposed docking pose of 5c (yellow) and EGCG (green) with Aβ42 peptide showing pro-posed binding interactions.

67x29mm (300 x 300 DPI)

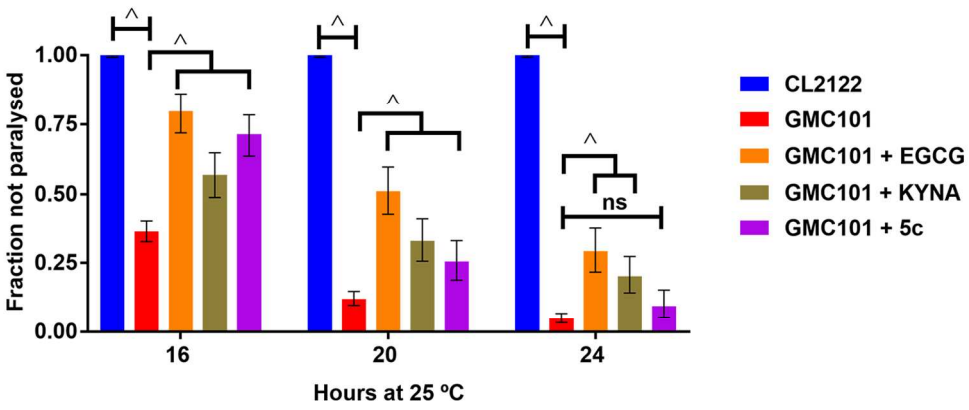

Figure 4. Protection against Aβ42-induced toxicity in C. elegans at 25 oC. Plotted are the proportions of individuals not paralysed for untreated strains GMC101 and CL2122, and GMC101 grown in a Petri dish (30 mm x 15 mm) on media that was pre-treated with 100 µL of 2 mM of 5c, KYNA and EGCG. Values are the mean with upper and lower 95% confidence intervals, based on data pooled from three independent experiments: Control strain CL2122 (n = 487),50 Aβ42 strain GMC101 (n = 678),50 GMC101 strain + 5c (n = 157), GMC101 strain + KYNA (n = 158), GMC101 strain + EGCG (n = 137),50 where n = number of individuals assayed. Statis-tical significance was determined by a 5×2 Fisher's exact test, which gave an overall P value < 0.001. A series of 2×2 Fisher's exact tests were subsequently conducted for pairwise comparisons, applying the Bonferroni correction for multiple tests, with ^P < 0.007.

127x54mm (300 x 300 DPI)

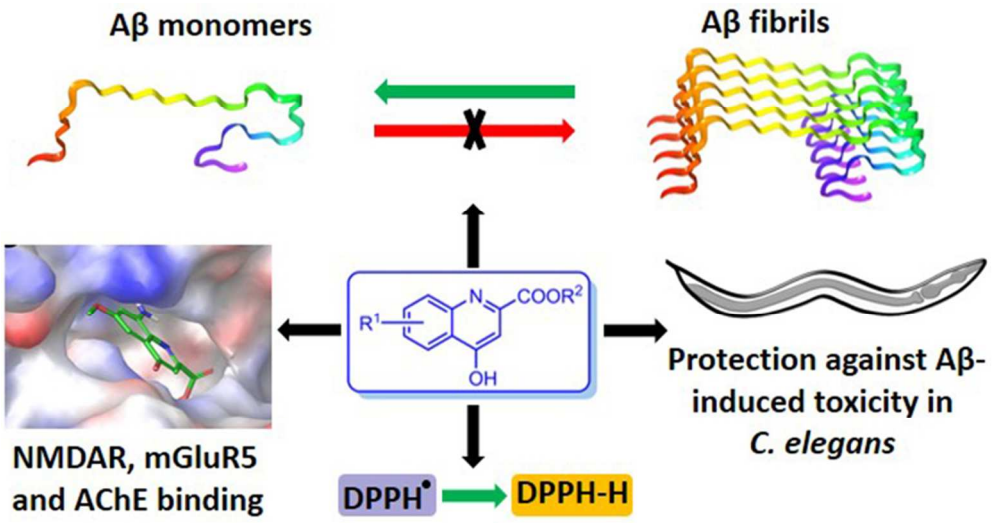

TOC Graphic

75x39mm (300 x 300 DPI)